

Discovery of Inhibitors of *Schistosoma mansoni* HDAC8 by Combining Homology Modeling, Virtual Screening, and in Vitro Validation

Srinivasaraghavan Kannan,^{†,‡} Jelena Melesina,[†] Alexander-Thomas Hauser,[‡] Alokta Chakrabarti,[‡] Tino Heimburg,[†] Karin Schmidtkunz,[‡] Alexandra Walter,^{‡,§,||} Martin Marek,[⊥] Raymond J. Pierce,[○] Christophe Romier,[⊥] Manfred Jung,[‡] and Wolfgang Sippel*,[†]

[†]Department of Pharmaceutical Chemistry, University Halle-Wittenberg, 06120 Halle/Saale, Germany

[‡]Institute of Pharmaceutical Sciences, University of Freiburg, 79104 Freiburg, Germany

[§]German Cancer Consortium (DKTK) 79104 Freiburg, Germany

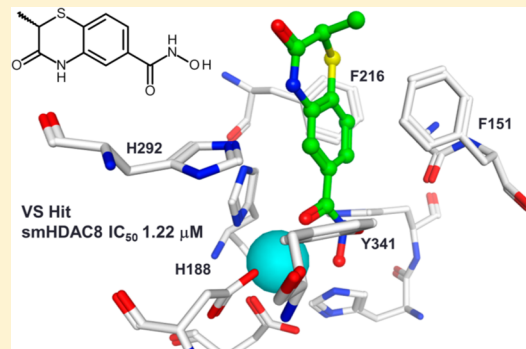
^{||}German Cancer Research Center (DKFZ), 69121 Heidelberg, Germany

[⊥]Département de Biologie Structurale Intégrative, Institut de Génétique et Biologie Moléculaire et Cellulaire (IGBMC), Université de Strasbourg (UDS), CNRS, INSERM, 1 rue Laurent Fries, B.P. 10142, 67404 Illkirch Cedex IGBMC, France

[○]Center for Infection and Immunity of Lille (CII), INSERM U1019—CNRS UMR 8204, Université Lille Nord de France, Institut Pasteur de Lille, 1 rue Professeur Calmette, 59019 Lille Cedex, France

Supporting Information

ABSTRACT: Schistosomiasis, caused by *S. mansoni*, is a tropical disease that affects over 200 million people worldwide. A novel approach for targeting eukaryotic parasites is to tackle their dynamic epigenetic machinery that is necessary for the extensive phenotypic changes during their life cycle. We recently identified *S. mansoni* histone deacetylase 8 (smHDAC8) as a potential target for antiparasitic therapy. Here we present results from a virtual screening campaign on smHDAC8. Besides hydroxamates, several sulfonamide-thiazole derivatives were identified by a target-based virtual screening using a homology model of smHDAC8. In vitro testing of 75 compounds identified 8 hydroxamates as potent and lead-like inhibitors of the parasitic HDAC8. Solving of the crystal structure of smHDAC8 with two of the virtual screening hits confirmed the predicted binding mode.



INTRODUCTION

Schistosomiasis, also called bilharzia, is one of the neglected, major human parasitic diseases; it is caused by small flat worm parasites from the genus *Schistosoma*.^{1,2} Schistosomes infect around 200 million people worldwide and cause at least 300 000 deaths yearly, with about 800 million people further at risk of infection.^{3,4} The treatment and control of schistosomiasis currently relies on one drug (praziquantel) which over decades has proven to be effective against all major schistosome species causing the disease. However, reduced efficiency of this drug as well as observed resistance in laboratory strains raise the specter of widespread drug resistance.^{5,8} Such drug resistance represents an increasing problem especially for parasitic diseases for which only a limited number of drugs is available for treatment. Thus, the search for potential drug targets and drug candidates against eukaryotic parasites is acute, notably for the major human parasitic diseases⁹ for which no effective vaccines are available.

The current success observed in targeting the human epigenome for the development of anticancer drugs has

broad implications notably concerning the discovery of novel drugs to cure human parasitic diseases that cause millions of deaths annually. Epigenetics refer to heritable changes in gene expression that occur without changes in the DNA sequence.¹⁰ These heritable changes are achieved by different post-translational modifications like methylation, phosphorylation, ubiquitylation, and acetylation of histone tails that determine the active or repressed state of chromatin.^{11,12} Although all these modifications contribute to the epigenetic gene regulation, two of these modifications, i.e. acetylation of lysine residues and the methylation of lysine or arginine residues of the tails of histones, seem to be particularly important in affecting the higher order structure of the chromatin fiber and in the consequent regulation of transcription.¹³ Histone modifying enzymes (HMEs) that are responsible for post-translational modifications are increasingly being reported as drug (therapeutic) targets for multiple diseases such as cancer,

Received: July 29, 2014

Published: September 22, 2014

inflammation, metabolic diseases, and neuropsychiatric disorders as well as in regenerative medicine.^{14–16}

One of the best investigated post-translational modifications is the deacetylation of the ϵ -amino group of lysine residues in histone tails and many nonhistone proteins. The process of acetylation and deacetylation is controlled by two families of enzymes; histone acetyl transferases (HATs) and the histone deacetylases (HDACs), respectively. Equilibrium between the activities of HATs and HDACs must be maintained for proper transcriptional activity and cellular function.¹⁷ In addition an increasing number of nonhistone proteins are recognized as substrates of HDACs, including those involved in transcription complexes, which play a pivotal role in the regulation of gene expression as well as cell proliferation, migration, death, and angiogenesis.¹⁸

HDACs are a family of enzymes found in numerous organisms including bacteria, fungi, plants, and animals that catalyze removal of acetyl groups from acetylated lysine residues of various protein substrates such as histones, transcription factors, alpha-tubulin, and nuclear importers. So far, 18 different members of HDACs have been discovered in humans and have been grouped into 4 classes based on their homology to yeast histone deacetylases.¹⁹ Class I consists of four different subtypes (HDAC1, 2, 3, and 8) and represents homology to the yeast protein RPD3; Class II includes six subtypes which are divided into two subclasses, Class IIa with subtypes HDAC4, 5, 7, and 9, and Class IIb with HDAC6 and 10. HDAC11 is referred to as Class IV. While the activity of Classes I, II, and IV HDACs depends on a zinc based catalysis mechanism, the Class III enzymes, also called sirtuins, require nicotinamide adenine dinucleotide as a cofactor for their catalysis. Seven different members (Sirt1–7) of NAD⁺-dependent HDACs have been discovered in humans so far,²⁰ and together they show homology to the yeast protein Sir2.

HDACs represent promising therapeutic targets in anticancer as well as antiviral, antiparasitic, and anti-inflammatory indications.^{21–24} HDAC inhibition has been shown to repress the transcription of tumor suppressor genes associated with the progression of various leukemia diseases.²⁵ There has been a considerable effort to develop HDAC inhibitors (HDACi); a number are in clinical trials and three are currently approved by the FDA for the treatment of cancer.²⁶

Recent investigations^{14,15,27,28} have shown that eukaryotic parasites possess HAT and HDAC orthologues and that the reversible acetylation seems to play a key role in gene transcriptional regulation and cell cycle progression. The potential antiparasitic activity of HDAC inhibitors was first shown for the cyclic tetrapeptide apicidin.²⁷ Since then, several studies using various HDACi have demonstrated the antiproliferative (anti parasitic) activity of these inhibitors on major human parasitic diseases such as leishmaniasis, malaria, schistosomiasis, toxoplasmosis, and trypanosomiasis.^{14,15}

In a previous study, we identified and characterized three class I HDACs present in the *Schistosoma mansoni* genome, orthologues to mammalian HDAC1, 3, and 8.²⁸ Treatment of smHDACs with generic HDAC inhibitors caused protein acetylation in schistosomes and dose-dependent mortality of schistosomula and adult worms.²⁹ Importantly, all three *S. mansoni* class I HDACs (smHDAC1, 3, and 8) are expressed at all life-cycle stages, with HDAC8 transcripts being always the most abundant,²⁹ indicating that this latter enzyme is most likely a major target for the design of schistosome specific inhibitors. These studies^{28–30} on *S. mansoni* and other parasites

uncovered the essential function of HDACs in the development and survival of the parasitic organism and revealed their potential as novel therapeutic target. Therefore, therapy with small-molecule HDAC inhibitors represents a promising approach for the treatment of schistosomiasis.

However, there are several challenges to overcome in order to develop drugs based on inhibitors of these enzymes. Given the degree of homology between members of this large family of enzymes, pharmacological inhibitors may have limited selectivity or specificity leading to toxicity against normal tissues. Several studies^{14,15} have highlighted the risk of cross-reactivity of developed drugs with host (human) enzymes that can cause off-target effects. Thus, in order to minimize these side effects the inhibitors have to be made as specific as possible for the schistosome enzymes.

In order to identify inhibitors of smHDAC8, we used a synergistic approach that combines the benefits of structure-based virtual screening and experimental testing with validated enzyme inhibition assays to subsequently screen only a limited number of compounds. As the crystal structure of any of class I *Schistosoma* HDAC enzymes was not available at the beginning of the project, a homology model of smHDAC8 was generated first. The smHDAC8 model was then used to virtually screen commercially available compound libraries. Compounds that were successfully docked were visualized for their interaction with the catalytic zinc ion and special importance was given for compounds that could make use of unique specificities in the active site of smHDAC8. A group of 75 compounds were selected and tested in a biochemical *in vitro* assay. During the course of our studies we were able to solve the X-ray structure of smHDAC8 in apo and ligand-inhibited form.^{31,32} The accuracy of the generated smHDAC8 homology model was further verified by comparing the model with the corresponding crystal structures. The structural flexibility of the residues at the active site of human and smHDAC8 was studied by means of molecular dynamics (MD) simulations. In addition the protein structures were subjected to Hamiltonian based replica exchange MD to further enhance the sampling.

In summary, our target based screening yielded promising lead-like hits that inhibit the *Schistosoma* enzyme and can be used as starting point for structure based optimization.

MATERIALS AND METHODS

Homology Modeling. A homology model of smHDAC8 was constructed using comparative modeling, by comparing the sequence of this target protein with sequences of other proteins (template) for which experimental structures are available. The sequences of smHDAC8 and human HDAC8 (hmHDAC8) were obtained from the Uniprot database (Uniprot ID: ASH660 and Q9BY41). A BLAST search was carried out with the protein data bank database for identification of a template structure. The full length sequence of smHDAC8 with 440 amino acids was used as query sequence in the BLAST search. An initial BLAST search showed that the sequence of smHDAC8 shares 40% sequence identity with hmHDAC8 and sequence alignment between the two reveals that this sequence similarity is distributed throughout the sequence with seven insertions in the sequence of smHDAC8 (Figure S1). Twenty-one crystal structures have been reported for hmHDAC8 in complex with inhibitors (PDB ID: 1T64, 1T67, 1T69, 2V5W, 1VKG, 1W22, 2VSX, 3EW8, 3EWF, 3EZP, 3EZT, 3F06, 3F07, 3FOR, 3MZ3, 3MZ4, 3MZ6, 3MZ7, 3RQD, 3SFF, 3SFH). Based on the resolution values, the crystal structure of

Table 1. Docking Scores and in Vitro Data of 75 Compounds Identified by Virtual Screening^a

cpd	supplier	class	GlideSP HM	GlideSP Xray	Gold GS	Gold CS	Gold PLP	Gold ASP	% inhib on plate	% inhib 25 μ M	% inhib 10 μ M	% inhib at $x \mu$ M	IC_{50}
S144030	Chembridge	hydroxamate	-7.87	-7.97	47.58	24.98	39.84	39.22	n.i.				
S158497	Chembridge	hydroxamate	-8.50	-8.38	54.99	36.00	61.32	50.12	69	18	4.4		
S234974	Chembridge	hydroxamate	-7.97	-7.00	42.27	34.46	45.15	43.78	42	25.3	19.7		
S808200	Chembridge	hydroxamate	-7.55	-7.48	51.24	26.01	43.80	37.23	n.i.				
S809354	Chembridge	hydroxamate	-5.62	-5.55	52.01	29.96	53.85	40.97	43				
6022898	Chembridge	hydroxamate	-4.77	-4.45	50.11	26.23	44.18	37.97	24				
8016-7993	ChemDiv	hydroxamate	-8.31	-7.78	49.51	27.42	26.46	38.40	37				
AmbtbhD1273	Ambinter	hydroxamate	-8.73	-9.06	43.86	27.47	30.08	32.41	n.i.				
F2502-0022	LifeChemicals	hydroxamate	-5.90	-6.60	52.36	26.31	40.96	44.01	87	60.7	36.8		
F2502-0023	LifeChemicals	hydroxamate	-7.77	-7.86	54.49	27.96	34.72	41.60	75	44.9	22.2		
F2502-0026	LifeChemicals	hydroxamate	-7.61	-8.54	53.71	26.96	38.97	46.39	77	46	24.7		
F2502-0041	LifeChemicals	hydroxamate	-8.05	-7.55	56.18	29.37	51.41	41.20	38				
F2502-0052	LifeChemicals	hydroxamate	-7.99	-7.41	62.28	31.93	71.02	58.41	52	24.7	10.6		
F2502-0071	LifeChemicals	hydroxamate	-8.56	-7.41	62.59	25.98	82.46	60.48	24				
F2502-0127	LifeChemicals	hydroxamate	-7.36	-7.01	59.73	22.35	49.59	40.75	52	29.7	28.6		
F2502-0137	LifeChemicals	hydroxamate	-7.25	-7.55	55.76	23.18	53.82	43.87	32				
F2502-0146	LifeChemicals	hydroxamate	-7.27	-7.15	53.80	21.62	34.70	39.24	17				
K783-2573	ChemDiv	hydroxamate	-8.37	-7.90	62.23	26.06	13.65	25.79	14		14.1		
K783-3535	ChemDiv	hydroxamate	-8.88	-7.84	68.18	49.49	71.81	57.43	n.i.				
K783-3536	ChemDiv	hydroxamate	-8.39	-8.27	66.03	47.31	62.79	59.39	n.i.				
K783-3540	ChemDiv	hydroxamate	-8.64	-8.41	69.10	46.91	59.02	54.62	n.i.				
K783-3776	ChemDiv	hydroxamate	-9.22	-8.06	65.78	43.82	73.97	60.17	n.i.				
K783-3793	ChemDiv	hydroxamate	-9.09	-7.47	65.16	43.30	53.39	47.88	89		35.8 (3.9 μ M)	21.3 ± 5.08	
K783-3795	ChemDiv	hydroxamate	-8.83	-8.13	63.50	47.08	40.97	50.50	n.i.				
K783-3809	ChemDiv	hydroxamate	-9.01	-8.24	63.37	44.20	44.03	51.39	38				
K783-3813	ChemDiv	hydroxamate	-9.03	-8.18	62.22	48.58	64.26	52.29	40		31.6 (4.1 μ M)	19.39 ± 6.5	
K783-3814	ChemDiv	hydroxamate	-9.23	-8.51	62.19	41.99	82.92	58.56	n.i.				
K783-3815	ChemDiv	hydroxamate	-8.95	-8.44	65.56	46.66	77.36	63.13	50				
K783-3816	ChemDiv	hydroxamate	-9.00	-8.03	64.86	46.27	36.85	33.84	82		53.1 (3.8 μ M)	6.5 ± 2.08	
K783-3824	ChemDiv	hydroxamate	-8.60	-7.71	62.92	48.38	84.70	61.78	n.i.				
KM00883	Maybridge	hydroxamate	-4.16	-4.11	39.42	33.30	13.15	43.97	n.i.				
KM02107	Maybridge	hydroxamate	-7.99	-8.00	55.21	25.83	28.05	30.49	n.i.				
KM04276	Maybridge	hydroxamate	-8.10	-6.08	50.16	20.18	53.44	38.96	n.i.				
OSSK 288845	Princeton	hydroxamate	-8.50	-8.82	51.91	30.89	25.42	44.16	n.i.				
OSSK 322582	Princeton	hydroxamate	-7.69	-5.67	51.14	27.22	41.85	37.70	64		24.5 (8.6 μ M)		
OSSK 799881	Princeton	hydroxamate	-8.07	-8.25	43.24	26.34	22.17	38.80	n.i.				
OSSK 927021	Princeton	hydroxamate	-4.57	-3.97	49.46	44.16	23.77	35.80	n.i.				
OSSK 927048	Princeton	hydroxamate	-4.12	-3.81	35.90	33.66	23.61	37.83	n.i.				
OSSL 166891	Princeton	hydroxamate	-6.98	-7.67	59.06	29.69	39.49	48.78	60		17.0 (4.5 μ M)		
OSSK 552295	Princeton	hydroxamate	-8.86	-8.55	54.27	23.47	45.40	40.58	92	61.4	32.1		
OSSL 052099	Princeton	hydroxamate	-6.50	-7.04	50.22	14.53	22.84	35.66	n.i.				
OSSL 166884	Princeton	hydroxamate	-7.03	-7.83	53.33	13.67	45.57	42.67	67		21.4 (5.7 μ M)		
T5971079	Enamine	hydroxamate	-9.77	-9.03	44.79	31.04	54.17	42.66	98		3.16 ± 0.45		
T5979345	Enamine	hydroxamate	-9.24	-8.67	45.03	29.69	40.73	39.46	73		5.82 ± 0.72		
T6072858	Enamine	hydroxamate	-8.04	-8.31	48.07	30.50	42.73	35.21		63.9	54.7 ± 4.23		
Tubastatin A	SigmaAldrich	hydroxamate	-8.07	-9.39	57.34	43.86	71.98	54.20		61.6	9.62 ± 1.07		
Z59183211	Enamine	hydroxamate	-8.06	-8.53	42.20	33.07	21.56	43.91		33.8			
Z59183341	Enamine	hydroxamate	-7.20	-9.37	57.29	37.07	48.73	54.62		18.7			
Z59183588	Enamine	hydroxamate	-7.12	-8.33	60.14	30.63	73.99	55.51		21.9			
Z59183779	Enamine	hydroxamate	-7.83	-9.27	46.78	30.93	52.40	53.89		61.5			
Z59184147	Enamine	hydroxamate	-7.47	-8.72	72.71	33.75	47.75	37.04		53.3	5.18 ± 4.83		
OSSK 151589	Princeton	thiazole	-6.20	-5.66	39.72	39.45	16.17	41.65	n.i.				
OSSK 344407	Princeton	thiazole	-6.95	-5.91	57.11	38.04	56.30	41.90	n.i.				
OSSK 579511	Princeton	thiazole	-6.11	-5.71	55.57	43.55	30.08	54.75	n.i.				
OSSK 714197	Princeton	thiazole	-5.59	-5.38	42.27	34.90	16.73	44.71	13		14.0 (3.5 μ M)		

Table 1. continued

cpd	supplier	class	GlideSP HM	GlideSP Xray	Gold GS	Gold CS	Gold PLP	Gold ASP	% inhib on plate	% inhib 25 μ M	% inhib 10 μ M	% inhib at $x \mu$ M	IC_{50}
OSSK 775345	Princeton	thiazole	-5.04	-5.58	37.28	28.54	34.18	37.99	n.i.				
OSSK 897817	Princeton	thiazole	-8.02	-7.13	50.27	23.01	22.72	39.11	n.i.				
OSSK 929477	Princeton	thiazole	-5.28	-4.58	38.86	34.50	25.65	35.19	n.i.				
OSSK 012279	Princeton	thiazole	-4.00	-5.17	47.60	36.68	37.56	42.01	n.i.				
OSSK 013880	Princeton	thiazole	-4.36	-4.85	40.00	37.30	40.11	11.25	n.i.				
OSSK 285890	Princeton	thiazole	-5.46	-4.77	48.09	37.83	21.44	35.09	n.i.				
OSSK 371176	Princeton	thiazole	-7.11	-8.78	48.85	34.11	23.47	42.24	n.i.				
OSSK 373203	Princeton	thiazole	-7.95	-5.41	47.46	26.67	47.31	30.68	n.i.				
OSSK 392474	Princeton	thiazole	-4.69	-7.69	46.13	32.83	12.50	35.09	n.i.				
OSSL 093883	Princeton	thiazole	-7.96	-8.08	60.56	22.43	38.15	35.27	n.i.				
OSSL 096660	Princeton	thiazole	-7.81	-7.13	42.23	31.19	14.52	32.35	n.i.				
OSSL 148947	Princeton	thiazole	-6.88	-5.46	65.72	32.52	40.56	41.90	46				28.5 (9.1 μ M)
OSSL 266957	Princeton	thiazole	-7.74	-7.49	50.19	20.42	23.54	32.65	n.i.				
OSSL 180907	Princeton	thiazole	-6.95	-5.16	48.87	33.99	24.97	36.81	38				
T05175810	Enamine	thiazole	-5.27	-5.18	53.41	37.15	26.26	37.96	35				
T5241370	Enamine	thiazole	-5.07	-5.50	55.80	34.99	36.79	38.06	n.i.				
T5254435	Enamine	thiazole	-5.30	-5.20	51.55	36.75	31.23	38.26	n.i.				
T5313533	Enamine	thiazole	-4.98	-5.19	62.72	38.37	35.38	43.38	n.i.				
7778127	Chembridge	aniline	-4.88	-4.60	34.90	39.84	21.74	40.60	n.i.				
8879700	Chembridge	aniline	-4.93	-4.66	38.09	38.83	18.54	38.52	n.i.				

^aThe table is sorted according to the chemical classes (hydroxamates, thiazoles, and anilines) and suppliers of the compounds. Docking scores derived using the smHDAC8 homology model (HM, GlideSP, Goldscore GS, Chemscore CS, Gold PLP score, and Gold ASP score) are shown. In addition the GlideSP score derived for the smHDAC8 X-ray structure (GlideSP Xray) is indicated. Primary inhibition on plate was tested at a concentration of 16.6 μ g mL⁻¹ using ZMTFAL. Detected hits were further tested at different concentrations using the same substrate.

hmHDAC8 bound with the inhibitor Trichostatin A (PDB ID 1T64)³³ was chosen as a template for the homology modeling. Modeler, a program for comparative protein structure modeling by satisfaction of spatial restraints³⁴ was used for generation of the homology model. Initially ten models were built based on structural information from the template. Superposition of the ten models revealed that the secondary structural elements of these models are quite similar; however, they all differ in the six loops regions, which corresponds to the insertions in the smHDAC8. Because of absence of structural information for these loop regions in the template structure, it was necessary to further refine the loop regions to obtain a stable and reliable model of smHDAC8. Again Modeler was used for modeling the loop regions and the structure with lowest DOPE score among the ten generated models was used as starting model for loop modeling. The variable loops were modeled one by one and for each loop, five models (only loop models) were generated and the loop model with lowest DOPE score was selected and used as starting structure for modeling of the next loop. Likewise a complete model of smHDAC8 was generated by using hmHDAC8 as template and further loop refinement using Modeler.

Similarly a homology model of the catalytic domains of human HDAC6 (hmHDAC6) was constructed using the X-ray structure of human HDAC4 (PDB ID: 4CBT)³⁵ as a template. Models of both catalytic domains of hmHDAC6 were constructed in a similar manner as smHDAC8, but without additional loop refinement.

Molecular Dynamics Simulation. The generated homology model of smHDAC8 was subjected to Molecular Dynamics (MD) simulations. The coordination of the zinc ion was taken from the hmHDAC8 structure after superimposing the model onto the human structure. MD simulations were carried using

the program AMBER11.³⁶ The Xleap module was used to prepare the system for MD simulations. Hydrogen atoms were added to all amino acids assuming a normal ionization state for all ionizable residues. Fourteen Na⁺ counterions were added to neutralize the system. Then the system was solvated in an octahedral box with TIP3P³⁷ water molecules leaving at least 10 Å between the solute atoms and the borders of the box. An all atom version of ff03 force field³⁸ and a nonbonded model³⁹ for protein and zinc ion were used. Solvent molecules, counterions, and zinc ion were initially relaxed by means of energy minimization with restraints on the protein atoms. Then the whole system was energy minimized to remove any steric clash in the initial geometry of the protein. Subsequently, the system was gradually heated from 50 to 300 K with positional restraints (force constant: 50 kcal mol⁻¹ Å⁻²) on protein atoms over a period of 0.25 ns allowing water molecules and ions to move freely. A 9 Å cutoff for the short-range nonbonded interactions was used in combination with the particle mesh Ewald option⁴⁰ using a grid spacing of ~0.9 Å to account for long-range electrostatic interactions. The Settle algorithm⁴¹ was used to constrain bond vibrations involving hydrogen atoms. A time step of 2 fs was used during simulations. During additional 0.25 ns the positional restraints were gradually reduced to allow finally unrestrained MD simulation of all atoms over a subsequent equilibration time of 2 ns. A 10 ns production MD run was carried out from this equilibrated structure and conformations were saved for every 4 (10) ps.

To further explore the conformational sampling/space of the HDACs enzymes, both the homology model of smHDAC8 and crystal structure of hmHDAC8 in its apo state were subjected to the advanced sampling method, Biassing Potential Replica Exchange MD(BP-REMD). The BP-REMD method is a Hamiltonian REMD method that employs a biasing potential

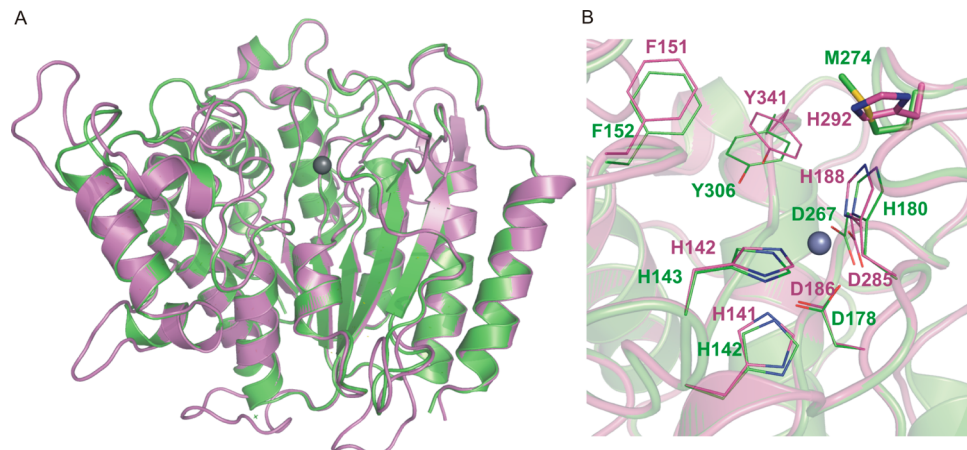


Figure 1. (A) smHDCA8 homology model (magenta) superimposed onto the hmHDAC8 crystal structure 1t64.pdb (green). The zinc ion is shown as a gray ball. (B) Important residues in the active site. The single substitution (M274 in human is replaced by H292) in smHDAC8 is highlighted in stick representation.

for the Φ and Ψ peptide backbone dihedral angles.⁴² Addition of the biasing potential during a simulation lowers the energy barriers for backbone dihedral transitions in a peptide or protein essentially making the protein chain more flexible. In the current work biasing potential replica exchange MD simulation with five replicas were carried out starting from the well equilibrated homology model, (at 300 K). BP-REMD simulations were carried out for 25 ns and exchanges between neighboring biasing levels were attempted every 2 ps (1000 MD steps) thus resulted in 12500 attempted exchanges with acceptance probability for replica exchange in the range of ~35%.

Virtual Screening. A docking protocol using the Glide⁴³ program was developed and validated by redocking the cocrystallized inhibitors (hydroxamates) of hmHDAC8 with its corresponding crystal structures. Ligands were prepared in MOE (2012.10, Chemical Computing Group, Montreal, Canada). Molecular docking was carried out using the Glide suite in the standard precision (SP) mode. Constraint to the Zn ion was used and conserved water molecules were considered in the docking run.

To evaluate the suitability of the generated homology model for docking studies, the cocrystallized inhibitors of hmHDAC8 were docked into the active site of smHDAC8. In all top-ranked docking poses the coordination between the hydroxamate and the zinc ion was obtained.

Then we screened the “ZINC drug-like” database⁴⁴ to identify novel inhibitors of smHDAC8. This database contains about 15 million compounds that are commercially available from different chemical suppliers. Using known zinc binding moieties (thiazoles, hydroxamates, and anilinobenzamides) as search query we identified ~5000 compounds and docked all of them into the active site of the smHDAC8 homology model using Glide with the protocol that was validated earlier. In the case of several stereoisomers generated for one compound the one that showed the best docking score was selected. The Glide docking solutions were rescored using different scoring functions (GlideSP,⁴⁵ GoldScore,⁴⁶ ChemScore,⁴⁷ ASP,⁴⁸ PLP⁴⁹). The top ranked solutions of each scoring were considered for further analysis (GlideSP < -7.0, GoldScore > 60, ChemScore > 30, PLP > 35, ASP > 35). In addition, the docking poses were visually inspected in MOE for their interaction with the catalytic zinc ion located in the smHDAC8

binding pocket. Based on availability 75 compounds were purchased from their corresponding suppliers and tested in an *in vitro* inhibition assay (Table 1).

During the course of the project, we solved the X-ray structures of smHDAC8 in complex with inhibitors.³¹ Therefore, the derived virtual screening hits and cocrystallized inhibitors were also docked into the active site of the crystal structure of smHDAC8 (PDB ID: 4BZ8) using the same protocol as previously used in the case of the homology model of smHDAC8. Docking scores of this experiment are shown in Table 1 in comparison to the scores derived by using the homology model.

Ligand Docking into Structures of Human HDACs.

During the initial biological screening on smHDAC8 the most promising hits (compounds K783-3816, T5971079, T5979345, T6072858, Z59184147, and Tubastatin A) were selected for further evaluation on human HDAC isoforms 1, 3, 6, and 8. Therefore, these compounds together with two reference compounds (SAHA and M344) were docked into X-ray structures of of human HDAC8 (PDB ID: 2V5X), HDAC1 (PDB ID: 4BKX), and HDAC3 (PDB ID: 4A69), as well as to homology models of the catalytic domains of human HDAC6 to explain the obtained biological data.

Activity and Inhibition Assays. Human and smHDAC8 activity testing was carried out with the HDAC8 Fluorimetric Drug Discovery Kit (Fluor de Lys(R)-HDAC8, BML-KI178) from Enzo Life Sciences according to the manufacturer’s instructions with a substrate concentration of 50 μ M. Fluorescence was measured in a plate reader (BMG Polarstar) with excitation at $\lambda = 390$ nm and emission at $\lambda = 460$ nm. Inhibition data for human HDACs 1, 3, and 6 were obtained according to published procedures with Z(Ac)Lys-AMC (ZMAL) as the substrate and trypsin as the developing agent.⁵⁰ HDAC1, 3, and 6 were purchased from BPS Bioscience.

Compounds were purchased from Ambinter (France), Chembridge (US), Chemdiv (US), Enamine (US), Life-Chemicals (US), Maybridge (US), Princeton (US), and Sigma-Aldrich (US) (Table 1).

For pretesting of smHDAC8 inhibition, a trypsin based assay setup was chosen that uses a trifluoroacetylated substrate Z(Tfa)Lys-AMC (ZMTFAL).⁵⁰ The assay was carried out in 96-half-well plates with a reaction volume of 30 μ L, containing

the fluorescent substrate ZMTFAL ($25 \mu\text{M}$), smHDAC8 preparation ($10 \mu\text{L}$) and the inhibitors in DMSO in varying concentrations ($2.5 \mu\text{L}$). After 90 min of incubation, the reaction was stopped by adding a solution that contains trypsin as developing agent. The resulting fluorescence was measured in a plate reader (BMG Polarstar) with an excitation wavelength of 390 nm and an emission wavelength of 460 nm . The amount of remaining substrate in the positive control with inhibitor versus negative control without inhibitor was employed to calculate inhibition. All determinations were carried out in duplicate.

RESULTS

Homology Modeling. The smHDAC8 model adopts a single alpha/beta domain in which several parallel beta sheets are sandwiched between alpha helices (Figure 1a). More than half of the amino acids constitute secondary structure elements and the rest correspond to loops that connect the secondary structure elements. Interestingly the *Schistosoma* specific insertions compared to their mammalian orthologues seen in the sequence alignment extend the external surface loops in the modeled structure. These extensions are located away from the active site, suggesting that they do not influence the catalytic mechanism directly and may form schistosome-specific protein/protein interaction surfaces. To evaluate the stability and for further refinement, the modeled smHDAC8 was subjected to molecular dynamics simulation. Root mean square deviation (rmsd) (Figure S2) of conformations sampled during the simulations show that the homology model reaches an equilibrium state at $\sim 2\text{--}3 \text{ ns}$ with a rmsd value of $\sim 2\text{--}2.5 \text{ \AA}$. Visual inspection of the trajectory revealed that the overall structure is highly stable with exceptions for certain loops that were found to be more flexible. The coordination of the zinc ion with active site residues was well maintained during the simulation. This was further verified by calculating the distances between the zinc ion and corresponding atoms in Asp186, Asp285, His188.

Comparison with Human HDAC8. Comparison of the generated homology model of smHDAC8 with its corresponding human isoform revealed that the catalytic domain of smHDAC8 bears a close resemblance to the crystal structure of hmHDAC8 showing an rmsd of $\sim 1 \text{ \AA}$ for the secondary structural elements (Figure 1a). However, considerable structural deviations were observed for the variable regions, especially for the schistosome-specific insertion regions. Structural comparison of smHDAC8 with hmHDAC8–inhibitor complexes reveals that the residues in the active site are very similar and therefore will have a similar interaction pattern with inhibitor and substrate. The active site of smHDAC8 consists of a long narrow tunnel leading to a cavity that contains the catalytic machinery at the end of this tunnel (Figure 1b). The residues that constitute the tunnel are mainly hydrophobic (Phe151, His188, Gly150, Phe216, His292, Tyr341) and are conserved within this HDAC class (except His292). The catalytic zinc ion which is deeply buried at the end of this catalytic tunnel in hmHDAC8 occupies the same position in human and smHDAC8 and shows the same coordination through interactions with Asp186, Asp285, and His188. Other residues that are important for the catalytic activities of hmHDAC8 are also structurally conserved in smHDAC8. A notable difference was found at the rim of active site in which Met274 in hmHDAC8 is substituted by His292 in smHDAC8 (Figure 1b). Replacement of Met274 by His292 in

smHDAC8 diminishes the hydrophobic character of the pocket that normally accommodates the aliphatic part of the incoming acetylated lysine. The presence of a polar residue replacing a hydrophobic one in the active site of smHDAC8 suggested a key feature that could be exploited to design smHDAC8-specific inhibitors.

Validation of the Docking Protocol by Docking of Known Inhibitors. A docking study was conducted to evaluate the predictive ability of the homology model and its suitability for use in structure based screening studies. A set of known human HDAC inhibitors all with a hydroxamate as the zinc chelating group was used for this study (Figure S3). Most of the HDAC inhibitors can be grouped into a simple pharmacophore model where a zinc-binding motif is connected via a linker to a more bulky capping group. Analysis of available three-dimensional structures of hmHDAC8s cocrystallized with hydroxamates revealed the relevant interactions. The hydroxamate moiety which acts as a zinc chelating group, coordinates with the zinc ion through its carbonyl and hydroxyl oxygens. It also interacts with residues His142, His143, and Tyr306 through hydrogen bonds. The same interaction pattern is observed in all crystal structures of HDAC8/hydroxamate complexes. However, considerable structural differences were observed for the capping groups of the inhibitors that interact with amino acids located at the rim of the channel (Figure S3). First the cocrystallized inhibitors were docked into their corresponding hmHDAC8 structures. The docked conformations of each ligand had rmsd values between 0.5 and 1.6 \AA with the corresponding experimental structure. In some poses only the capping group adopts different conformations. Using the same protocol, these hydroxamate derivatives were docked into the active site of smHDAC8. Visual inspection of the docked complexes reveals two major conformations of these inhibitors. The hydroxamate moiety in all docking poses coordinates with the zinc through its carbonyl and hydroxyl oxygen atoms. In addition, hydrogen bond interactions with the residues His141, His142, and Tyr341 can be observed (Figure 2). The linker region occupies the narrow tunnel and has lipophilic interactions with the residues from the tunnel region.

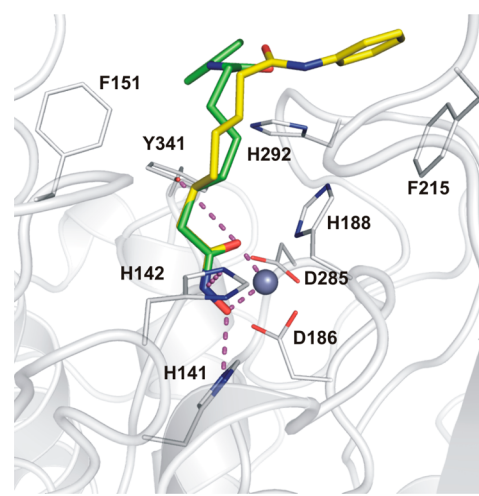


Figure 2. Docking poses of SAHA (green and yellow carbon) with two different orientations of the capping group, in the homology model of smHDAC8. Residues in the active site are shown in stick representation. The zinc ion is shown as blue ball and hydrogen bonds are indicated as dashed lines (magenta).

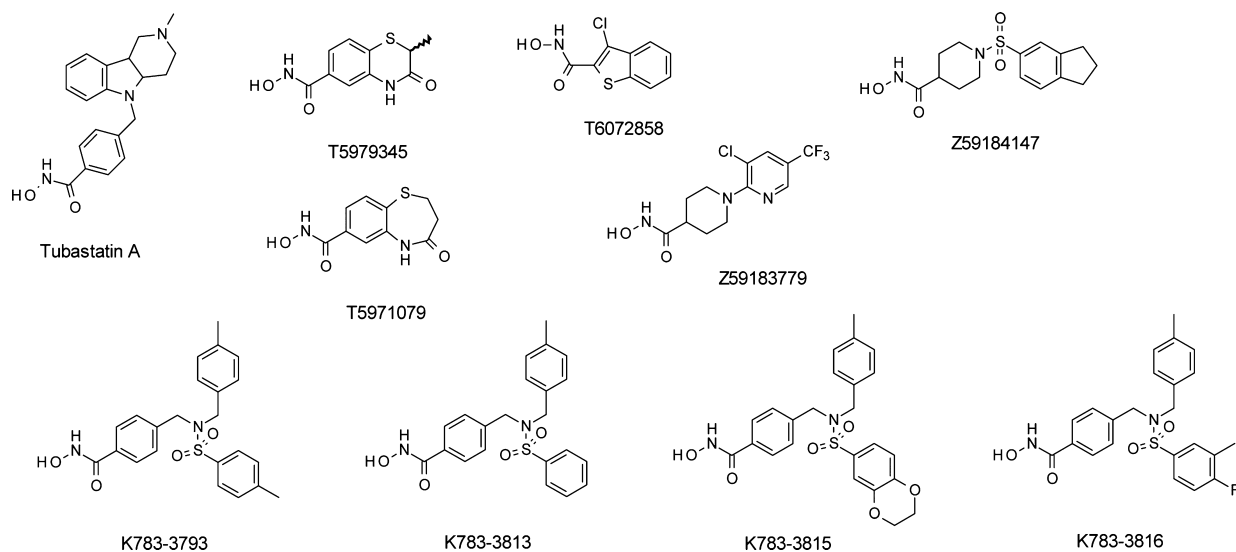


Figure 3. Chemical structure of the hits derived from the virtual screening.

Table 2. In Vitro Inhibition of smHDAC8 and Human HDACs Using Different Substrates

isofrom substrate	smHDAC8 ZMTFAL	smHDAC8 Fluor de Lys	hmHDAC8 ZMTFAL	hmHDAC8 Fluor de Lys	hmHDAC1 ZMAL	hmHDAC6 ZMAL	hmHDAC3 ZMAL
cpd	IC ₅₀ ± SE [μM]	IC ₅₀ ± SE [μM]	IC ₅₀ ± SE [μM]				
K783-3816	56.5% @ 50 μM ^b	5.63 ± 0.24	2.22 ± 0.11	1.35 ± 0.54	26.07 ± 3.24	0.42 ± 0.16	nd ^a
T5971079	3.16 ± 0.45	1.22 ± 0.28	2.46 ± 0.23	0.62 ± 0.08	9.78 ± 0.71	1.33 ± 0.18	12.46 ± 1.55
T5979345	5.82 ± 0.72	1.48 ± 0.46	6.3 ± 1.0	0.97 ± 0.11	27.48 ± 8.33	3.56 ± 0.55	12.31 ± 0.68
T6072858	54.7 ± 4.23	4.32 ± 0.29	2.79 ± 0.61	3.09 ± 0.55	11.65 ± 3.50 16.03 ± 3.05	1.88 ± 1.21	37.41 ± 4.88
Z59184147	33.1 ± 10.2	3.03 ± 0.61	10.6 ± 0.62	1.33 ± 0.66	6.74 ± 0.72	2.13 ± 0.59	nd
Tubastatin A	11.78 ± 2.57	1.48 ± 0.10	12.3 ± 3.60	1.30 ± 0.60	3.35 ± 0.51	0.02 ± 0.005	nd
SAHA	13.83 ± 2.40	1.56 ± 0.20	7.39 ± 0.5	0.40 ± 0.10	0.117 ± 0.006	0.042 ± 0.011 0.104 ± 0.009	0.155 ± 0.020 0.092 ± 0.097
M344	15.48 ± 1.27	3.14 ± 0.53	6.06 ± 1.06	0.33 ± 0.03	0.043 ± 0.005	0.018 ± 0.004	0.099 ± 0.013 0.065 ± 0.006

^aNot determined. ^bNot more than 60% inhibition was reached.

However, the capping group of these inhibitors had two different orientations. For example the phenyl ring in the cap of SAHA adopts two different orientations (Figure 2), interacting with Phe215 in one conformation and with Tyr341 in another docking pose.

Virtual Screening Identifies Novel smHDAC8 Inhibitors. In order to identify novel inhibitors for smHDAC8 we applied a virtual database screening strategy to conduct virtual screening with the drug like ZINC database. Our search was focused on compounds with chemical moieties that could act as zinc chelating groups. Among the 21 available human HDAC8-inhibitor crystal structures 16 of them contain hydroxamates and also a large number of hydroxamate based inhibitors are available in the literature. In addition, anilinobenzamides, or thiazole-sulfonamide groups are also shown to inhibit the activity of the human HDAC enzymes.⁴⁹ Therefore, the drug like ZINC database was screened for compounds containing hydroxamate, anilinobenzamides, or thiazole-sulfonamide groups which are known as zinc binding motifs.⁵¹ To end up with molecules that are likely to be more drug-like we used the following filters (MW below 500, logP below 4.0, TPSA below 140). About ~5000 compounds were retrieved and docked into

the smHDAC8 binding pocket. The final selection of a smaller subset of compounds (Figure 3) was based on the derived docking scores (Table 1) and a visual inspection of the predicted binding mode (see Methods part for details). Importance was given for compounds that could ideally coordinate to the zinc ion. Based on commercial availability, 75 compounds were purchased from different suppliers and tested in an in vitro assay for their ability to inhibit smHDAC8. Among the selected compounds, 51 hydroxamates, 22 thiazolo-sulfonamides, and 2 anilino-benzamides were purchased. The biological assay was carried out on microtiter plates using purified smHDAC8 protein and the small molecule substrate ZMTFAL^{50,52} which carries a trifluoroacetyl moiety. The pretesting in concentration between 3.5 and 25 μM resulted in 26 actives (25 hydroxamates and 1 thiazolo-sulfonamide; Table 2). The most active primary hits were further analyzed and IC₅₀ values were determined for eight compounds with the same trifluoroacetyl substrate that was used for pretesting as well a commercially available oligopeptide (Fluor de Lys) with an acetyl residue. The ZMTFAL substrate is less expensive and can be detected with trypsin whereas the Fluor de Lys kit is much more expensive. The exact nature of the developer

reagent is not revealed by the supplier. We wanted to compare ZMTFAL and Fluor de Lys for both sm and human HDAC8 in order to see the effect of the substrate on the inhibition. Usually the Fluor de Lys led to 5–10-fold lower IC_{50} values than ZMTFAL, but in some cases, very similar values were registered. So generally, Fluor de Lys might be substituted for larger prescreens by ZMTFAL but there is a chance that weaker inhibitors are missed. For human HDACs 1 and 6 ZMAL with an acetylated lysine is used, similar to many other studies before.^{50,52}

Among the active inhibitors we identified several linker-less aromatic hydroxamate derivatives including the known HDAC inhibitor Tubastatin A which inhibits smHDAC8 with an IC_{50} value of 1.48 μM (Fluor de Lys). The aromatic ring attached to the hydroxamate is surrounded by several residues of smHDAC8 (Phe151, Phe215, Phe216, His292, and Try341) forming an aromatic cone (Figure 4). Tubastatin A shows

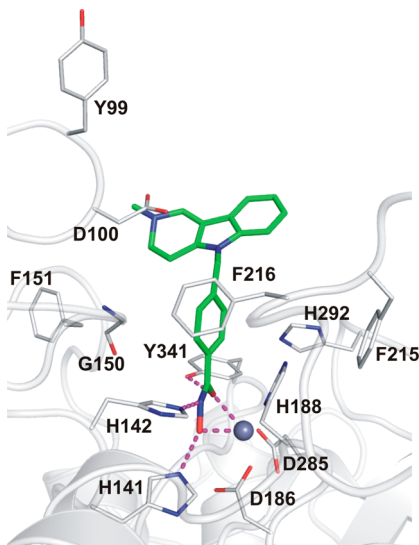


Figure 4. Docked pose of Tubastatin A (green carbon atoms) with the X-ray structure of smHDAC8 (PDB ID: 4BZ6). Residues in the active site are shown in stick representation. The zinc ion is shown as a blue ball, and hydrogen bonds are indicated as dashed lines (magenta).

similar inhibition of smHDAC8 as the two reference inhibitors we used in our in vitro assay (SAHA and M344, Table 2). All identified hydroxamates show the same coordination to the catalytic zinc ion as observed in the crystal structures of hmHDAC8 in complex with hydroxamates (interaction with His141, His142, and Tyr341).

The best Glide docking scores among the identified hits were observed for the two inhibitors T5971079 and T5979345 (-9.77 and -9.24 , respectively). Both compounds inhibit smHDAC8 in the low micromolar range (Table 2). Docking of these compounds to smHDAC8 revealed, that the nitrogen atom of the amide group of both inhibitors is involved in a hydrogen bond with His292 (Figure 5). Such a hydrogen bond interaction is not possible with hmHDAC8 and other isoforms where His292 is replaced by methionine and leucine. However, both inhibitors also inhibit hmHDAC8 at similar concentrations (Table 2). An explanation for the missing selectivity between human and parasite HDAC8 was found by docking the inhibitors into the human enzyme (discussed later).

T6072858, which contains a substituted benzothiophene, shows an IC_{50} value of 4.32 μM for smHDAC8 (Fluor de Lys).

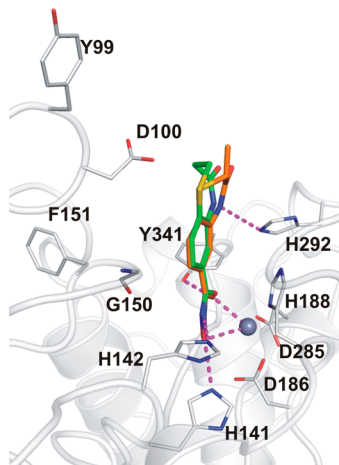


Figure 5. Docked pose of T5971079 (green carbon atoms) and T5979345 (orange carbon atoms) with the X-ray structure of smHDAC8 (PDB ID: 4BZ6). Residues in the active site are shown in stick representation. The zinc ion is shown as a blue ball, and hydrogen bonds are indicated as dashed lines (magenta).

In the docking solution the benzothiophene adopts a similar orientation as observed for the other aromatic hydroxamates (Figure 6). The fragment-like compound represents an

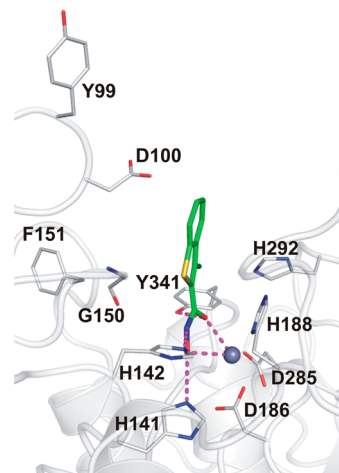


Figure 6. Docked pose of T6072858 (green carbon atoms) with the X-ray structure of smHDAC8 (PDB ID: 4BZ6). Residues in the active site are shown in stick representation. The zinc ion is shown as a blue ball, and hydrogen bonds are indicated as dashed lines (magenta).

interesting starting point for further structure-guided optimization because it also showed dose-dependent mortality of schistosomula and adult worms.³¹ The higher lipophilicity of this hit might be the reason for the observed cellular activity compared to the inactive compounds T5971079 and T5979345.³¹

A group of structurally similar inhibitors (K783-3793, K783-3813, K783-3815, and K783-3816), that are active in the low micromolar range, contains a substituted sulfonamide capping group which is attached by a methylene linker to an aromatic hydroxamate. The sulfonamide group is involved in a hydrogen bond with His188 whereas the two aromatic rings of the capping group interact with several hydrophobic and aromatic residues located at the rim of the pocket (Tyr99, Phe151, Phe215, Phe216, and Pro291; Figure 7). For the compounds of

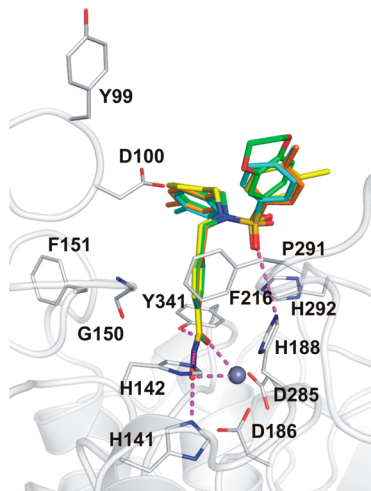


Figure 7. Docked poses of K783-3793 (yellow carbon), -3813 (cyan carbon atoms), -3815 (green carbon atoms), and -3816 (magenta carbon atoms) with the X-ray structure of smHDAC8 (PDB ID: 4BZ6). Residues in the active site are shown in stick representation. The zinc ion is shown as a blue ball, and hydrogen bonds are indicated as dashed lines (magenta).

this chemical series the rescoring showed the most favorable Goldscore (Table 1). Interestingly, some analogs of the same series were found to be inactive or weakly active. No structural explanation could be found for this effect on the basis of the docking and scoring results.

Two further inhibitors that were found to be active, Z59183779 (61% inhibition at 10 μ M, ZMTFAL) and Z59184147 (IC_{50} 3.03 μ M, Fluor de Lys), contain a piperidine connected to the hydroxamate instead of an aromatic ring system. The piperidine ring is further connected to a substituted sulfonamide or phenyl ring which interacts with the aromatic residues of the rim of the pocket as observed for K783-3816 (Figure 8).

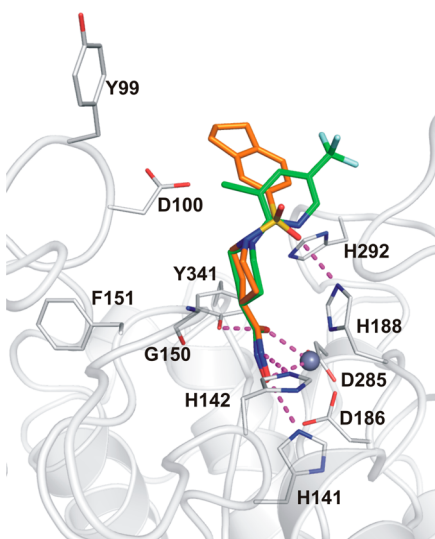


Figure 8. Docked poses of Z59183779 (green carbon atoms) and Z59184147 (orange carbon atoms) with the X-ray structure of smHDAC8 (PDB ID: 4BZ6). Residues in the active site are shown in stick representation. The zinc ion is shown as a blue ball, and hydrogen bonds are indicated as dashed lines (magenta).

The other zinc binding motifs did not result in strong inhibition of smHDAC8. Only the thiazolo-sulfonamide OSSL148947 showed 28.5% inhibition at a concentration of 9.1 μ M (ZMTFAL). The sulfonamide and the thiazole nitrogen atom coordinate the zinc ion as previously proposed in the work of Park et al.⁵¹ (Figure S4).

X-ray Structure of smHDAC8 and Comparison with the Homology Model. During the course of the project, we successfully solved the crystal structure of smHDAC8 in its apo form and bound with inhibitors. Besides the pan-HDAC inhibitor SAHA we were also able to cocrystallize the identified hits T5979345 and T6072858. The coordinates of all smHDAC8 structures have been recently published and details can be found there [PDB ID 4BZ5, 4BZ6, 4BZ7, 4BZ8, and 4BZ9].³¹ Comparison of the homology model with the crystal structure of smHDAC8 in its apo form, shows that the generated homology model is in good agreement with the crystal structure with rmsd of \sim 1.5 Å. The crystal structures are incomplete with structural information missing for four loop regions and these residues correspond to the insertions that were seen earlier in the sequence alignment. As seen in the homology model, the crystal structure of smHDAC8 also has the His292 at the rim of active site which corresponds to Met274 in human HDAC8 (as predicted by the model). The active site residues from both structures can be superimposed with an rmsd value of \sim 0.5 Å. Comparison of the homology model with the inhibitor bound structure reveals several notable differences between the modeled and crystal structures of smHDAC8.

The smHDAC8 crystal structure in complex with SAHA shows four identical monomers and all of them are bound to the inhibitor. The bound conformation of SAHA is highly similar in all monomers. Structural differences are observed when compared to the bound SAHA conformation in hmHDAC8 crystal structure (not shown). Also the protein structure is highly similar in all four monomers; however, a major difference can be seen for the conformation of Lys20. In monomer D Lys20 is flipped toward the binding site and makes a hydrogen bond interaction with Tyr341 and also with SAHA. In all other monomers Lys20 has a different conformation or is not unambiguously resolved. A notable difference was found in the entrance region of the binding tunnel. Phe151 (which corresponds to Phe152 in hmHDAC8) at the rim of the active site shows a different side chain orientation compared to the homology model (Figure 9). The side chain of the conserved Lys20 in smHDAC8 occupies the space that is occupied by Phe152 in the human structure and forces Phe151 in the smHDAC8 structure into a different orientation. Moreover, in one monomer of the smHDAC8 X-ray structure Lys20 interacts with SAHA through hydrogen bonding.

Despite having adopted different conformations for Phe151 and Lys20 in its apo and SAHA-bound states, the highest structural similarity especially for the conformations of Phe151 and Lys20 residues, between homology model and crystal structure was observed in the case of smHDAC8 complexed with T5979345 (PDB ID: 4BZ8). Interestingly in this smHDAC8 cocrystal structure the highly conserved residue Phe151 is flipped in and Lys20 attains a flipped out conformation that is similar to the conformation observed in the homology model of smHDAC8 and X-ray structures of hmHDACs. Phe151 in its flipped in conformation stabilizes the aromatic ring of the bound inhibitor. Moreover, the docking pose for T5979345 is exactly matching the observed position in

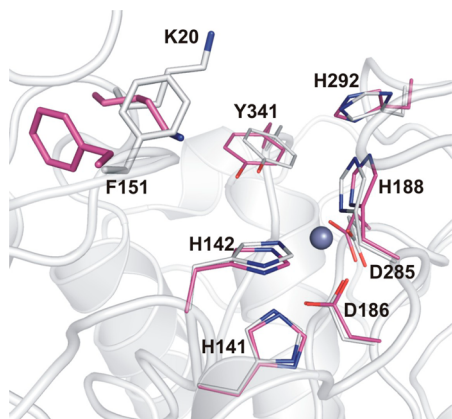


Figure 9. Superimposition of homology model of smHDAC8 (magenta) onto the crystal structure of SAHA bound smHDAC8 (PDB ID: 4BZ6, gray). The zinc ion is shown as a gray ball. Important residues in active site are shown in stick representation.

the cocrystal structure and shows the same interaction with His292 (Figure 10).

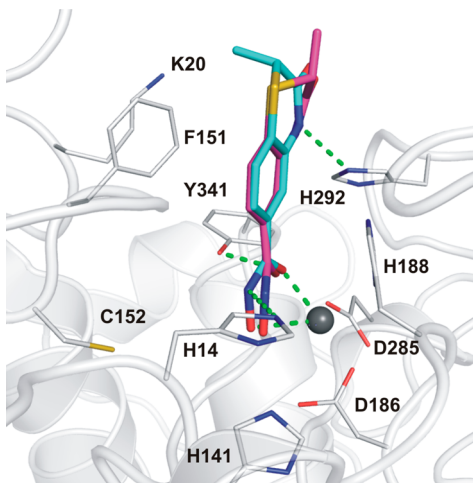


Figure 10. Comparison of Docked pose of T5979345 (cyan carbon atoms) into the homology model of smHDAC8 with its corresponding bound conformation in the cocrystal structure (PDB ID: 4BZ8) (magenta carbon atoms). Residues in the active site are shown in stick representation. The zinc ion is shown as a blue ball, and hydrogen bonds are indicated as dashed lines (green).

Since we recognized in the X-ray structures that Phe151 (as well as Lys20) is able to adopt different conformations in smHDAC8, we redocked all 75 tested compounds into the X-ray structure of smHDAC8 (in complex with SAHA, PDB ID: 4BZ6) where Phe151 is flipped out and Lys20 is pointing into the binding pocket. The docking poses of the active inhibitors were found to be similar to those obtained by docking to the homology model. The similar orientation of the aromatic ring of the hydroxamates can be explained by the interaction with Lys20. It adopts a similar orientation as the flipped in Phe151 in the homology model and the crystal structure in complex with T5979345 (PDB ID: 4BZ8) and stabilizes the aromatic ring by a π -cation interaction (Figure 10).

Docking into X-ray Structures of smHDAC8, Human HDAC8, HDAC1, and HDAC3 and into a Homology Model of Human HDAC6. The most interesting hits

identified by the in vitro testing were further tested on human and smHDAC8, as well as on human isoforms HDAC1, HDAC3, and HDAC6 (Table 2). To get insight into the selectivity of the identified inhibitors we docked the active inhibitors into the available structures of human HDAC1, HDAC3 (crystal structures), and HDAC6 (homology model). First we validated the docking protocol for these HDACs by using the known pan-HDAC inhibitor SAHA. In all docking models, the hydroxamate group is located in the HDAC binding pocket similar to its commonly observed binding mode in available HDAC X-ray structures. The binding pose of SAHA in human and smHDAC8 could be reproduced by the docking program with rmsd values of 1.7 and 2.0 Å, respectively. The docking poses of SAHA in hmHDAC1 and hmHDAC3 were similar to its binding pose in hmHDAC2 (PDB ID: 4LXZ) with rmsd values of 1.4 and 0.8 Å, respectively (Figure 11).

Compared to the high potency of SAHA and M344 on HDAC1 and HDAC3, the novel inhibitors showed reduced activity for these human isoforms. Docking to the novel X-ray structure of smHDAC8 and hmHDAC8, hmHDAC1, and hmHDAC3 as well as docking into the homology model of hmHDAC 6 showed, that this isoform selectivity could be explained by the narrower binding pocket channel of human HDAC1 and HDAC3 in comparison to human HDAC6, HDAC8, and smHDAC8. Ligands with fused ring linkers could not reach the zinc ion to chelate it, which is reflected by the distances between the oxygen atoms of the hydroxamate group and the metal atom (Table 3).

According to the virtual screening results, two compounds T5971079 and T5979345 make a hydrogen bond with the unique *S. mansoni* binding pocket residue His292. A similar interaction in hmHDAC8 is not possible due to presence of Met274 at this position. However, the biological data showed that there is no significant selectivity between these enzymes for the two compounds. An explanation for the missing selectivity between human and smHDAC8 was found by docking the inhibitors into both binding pockets including conserved water molecules. In hmHDAC8, a conserved water molecule bound to His180 interacts in a similar way with the two inhibitors as does His292 in smHDAC8. This interaction with the water molecule is also possible in hmHDAC1 and hmHDAC6 (Figure 12). T5979345 contains one chiral center in the lactam ring and was tested as racemic mixture. The docking of both stereoisomers resulted in similar docking poses and scores since the methyl group is not directly involved in an interaction with the protein.

Analysis of Enhanced Flexibility of smHDAC8 by Advanced Sampling Methods. The experimental structures of smHDAC8 revealed (two) different conformations for Phe151 and Lys20 (Figure 9) resulting in a different shape of the binding pocket. To understand the conformational flexibility of the residues in the active site of smHDAC8, the apo-structure was subjected to longer 25 ns MD simulations. In addition to the standard MD simulation, the recently developed Hamiltonian based replica exchange method named Biassing Potential Replica Exchange MD⁴² was used to further study the conformational sampling of active site residues by enhancing the conformational sampling during molecular dynamics simulations. To further compare the flexibility of the active site residues of smHDAC8 with the corresponding isoform in humans, the crystal structure of hmHDAC8 without a bound ligand was also subjected to MD and BP-REMD simulations. MD simulation of the uncomplexed smHDAC8 and

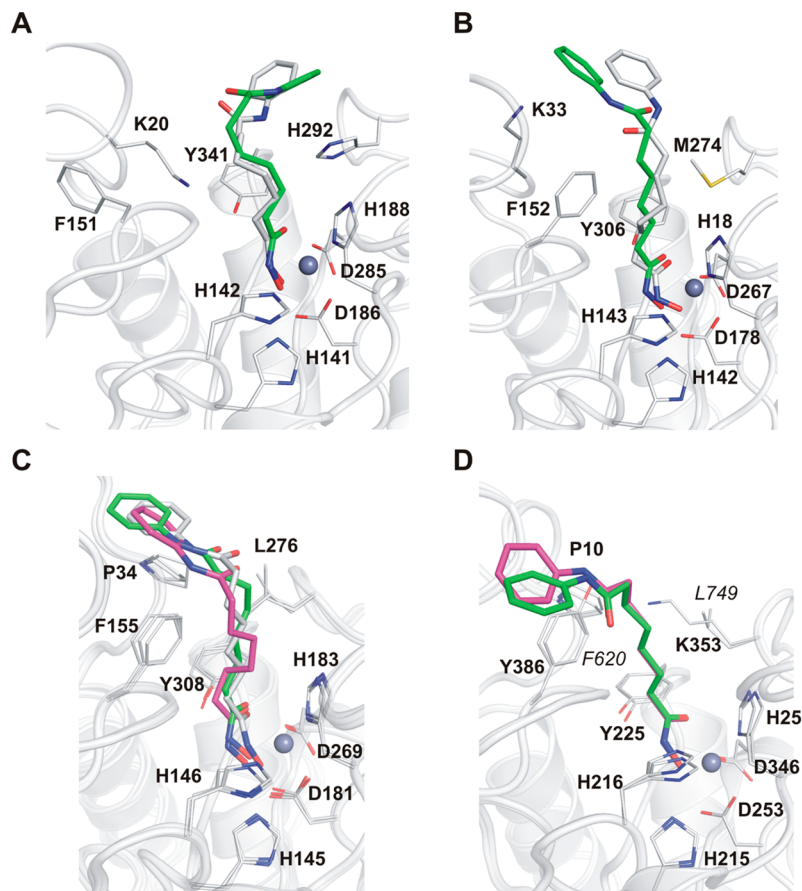


Figure 11. Docking poses of SAHA demonstrating the good coordination geometry of the hydroxamic acid with the zinc ion and surrounding residues: (A) comparison of docking pose of SAHA in smHDAC8 (green carbon atoms) with its binding pose (PDB ID: 4BZ6, gray); (B) comparison of docking pose of SAHA in hmHDAC8 (green carbon atoms) with its binding pose (PDB ID: 1T69, gray); (C) comparison of docking poses of SAHA in HDAC1 (green carbon atoms) and HDAC3 (magenta carbon atoms) with binding pose in HDAC2 (PDB ID: 4LXZ, gray); (D) docking pose of SAHA in homology models of both catalytic domains of HDAC6 (green and magenta carbon atoms). Conformations of SAHA and residues in the active site are shown in stick representation, and the backbone of the protein is shown as a ribbon. The zinc ion is shown as a gray ball.

Table 3. Average Distances (Å) between Oxygen Atoms of the Hydroxamate Group of the Docked Inhibitor and the Zinc Ion^a

	smHDAC8	hmHDAC8	hmHDAC1	hmHDAC6_1	hmHDAC6_2	hmHDAC3
T5971079	2.19	2.24	2.71	2.25	2.19	2.50
T5979345	2.11	2.03	2.87	2.24	2.21	2.59
T6072858	2.22	2.23	3.19	2.65	2.89	3.16
Z59184147	2.28	2.24	2.98	2.15	2.12	2.89
SAHA	2.01	2.27	2.30	2.31	2.27	2.34
M344	2.12	2.11	2.24	2.24	2.15	2.22

^aDistances equal to or larger than 2.5 Å are printed in bold font.

uncomplexed hmHDAC8 provides significant insights into the structural flexibility and dynamics of this protein in atomic details.

During the standard MD and BP-REMD simulations most of the active site residues of both the enzymes are highly stable, however, increased flexibility for some of the highly conserved active residues (Tyr341, Phe151, and Lys20) was observed during simulations of smHDAC8 (Figure 13). Notable structural differences were observed especially for residues Phe151 and Lys20 at the rim of the active site. Simulations were initiated from the crystal structure of smHDAC8 with Phe151 and Lys20 found in the out and in conformations, respectively. During the simulations, the side chain of Phe151 turned toward the active site and adopted a flipped in

conformation and Lys20 moved away from the active site and adopted a flipped out conformation that are similar to that of hmHDAC8 and in agreement with two different conformations observed in the cocrystal structures of smHDAC8. During the simulations, the flipping of the highly conserved residue Phe151 is coordinated with the movement of another highly conserved residue Lys20. In contrast during the simulations of hmHDAC8 in its uncomplexed state, such a flipping was not observed. Rather, the conformations of these two residues remain stable. The reduced flexibility observed for the active site residues during the simulations of hmHDAC8 showed that the coordinated movement of Phe152 and Lys20 is quite unique to smHDAC8, since Phe151 (Phe152 in human HDACs) is highly conserved across all isoforms of human HDACs (except

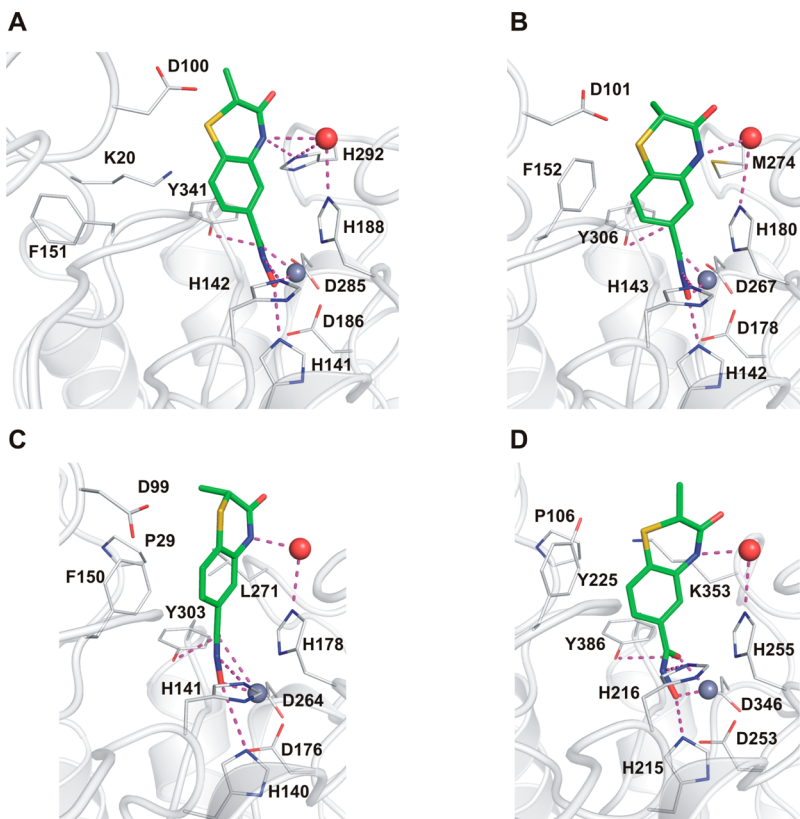


Figure 12. Docking poses of T5979345 in *S. mansoni* HDAC8 (A), human HDAC8 (B), HDAC1 (C), and first catalytic domain of HDAC6 (D). Residues in the active site are shown in stick representation, backbone of the protein are shown as ribbon. Water molecules are displayed as red balls, and the zinc ion is shown as a gray ball. Interactions between the zinc binding group of the docked ligand and the protein or water are shown as magenta lines.

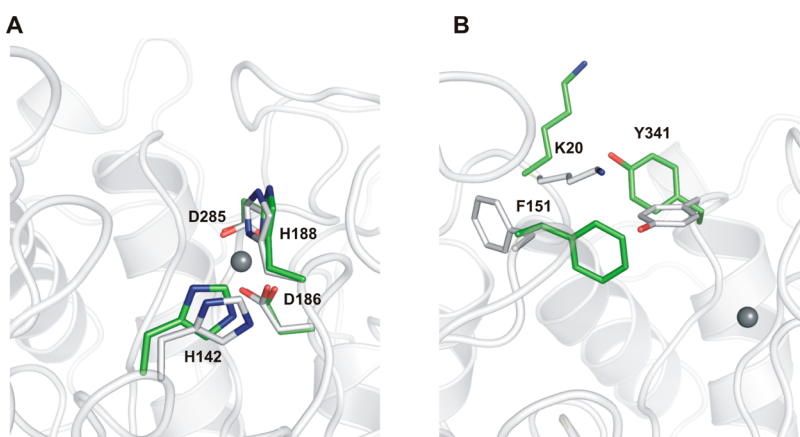


Figure 13. *Schistosoma* specific flexibility of catalytic (A) and noncatalytic (B) residues located in the active site, inferred from molecular dynamics simulations. Active site residues are show in stick representation with conformations at the start of simulation in (gray carbon atoms) and alternate conformation (green carbon atoms) sampled during the simulations.

HDAC6 where this is replaced by a tyrosine residue) and it is always found in a flipped in conformation. Thus, the flipped out conformation of Phe151 that is highly specific to smHDAC8 prevents this residue from participating in the formation of the narrow hydrophobic tunnel.

In addition, during smHDAC8 simulations increased flexibility was observed for residue Tyr341 that is located at the end of the narrow tunnel. Especially during BP-REMD simulations, the side chain of Tyr341 in smHDAC8 pointed toward the rim of the catalytic pocket and became solvent exposed. In contrast, the tyrosine residue at the similar position

in the human HDAC8 (Tyr306) was quite stable throughout the simulations, as seen in all the crystal structures of hmHDAC8 cocrystallized with hydroxamate inhibitors. In these cocrystal structures the hydroxyl group of the side chain of the highly conserved Tyr306 faces toward the zinc ion and interacts with the carboxyl group of the hydroxamate through a hydrogen bond, although a different conformation (similar to the one observed in the simulations of smHDAC8) for Tyr306 was observed in the two crystal structures of hmHDAC8 cocrystallized with nonhydroxamates. The subtle differences in conformational flexibility of smHDAC8 inferred

from our MD simulations will be considered in further virtual screening and optimization campaigns.

■ DISCUSSION

In order to identify inhibitors of smHDAC8, we used a synergistic approach that combines the benefits of structure-based virtual screening and experimental testing with validated HDAC inhibition assays to subsequently screen only a limited number of the top-ranking compounds. Despite of high sequence conservation of active site residues between human and smHDAC8, the homology model revealed a single substitution (Met274 to His292) at the rim of the binding site that modifies the shape and physicochemical properties of the smHDAC8 active site. This was later confirmed by the crystal structure of smHDAC8. Replacement of Met274 with a polar residue in parasitic HDAC8 increases the possibility of designing specific inhibitors.

At this initial step, a focused screen of only compounds that contain hydroxamates, hydroxamate derivatives, thiazolo-sulfonamides, and anilino-benzamides as zinc chelating groups from the ZINC database was carried out against the homology model of smHDAC8. Interestingly our structure-based virtual screening approach identified several linker-less aromatic hydroxamate derivatives. Naphthalene-2-hydroxamic acid has previously been shown to be a selective inhibitor of hmHDAC8.⁵³ Further docking of these compounds with the smHDAC8 model indicated that these compounds can make use of the smHDAC8 active site specificities that were identified from homology modeling.

Although these compounds are relatively potent against hmHDAC8, a significant loss in potency was observed for major human HDACs such as HDAC1 and HDAC3 as off-targets. This isoform specificity which could be explained by docking experiments makes these compounds interesting for further optimization, which should result in increased specificity toward smHDAC8 versus hmHDAC8.

To better understand the conformational flexibility of residues in the active site of smHDAC8 we carried out an all atom molecular dynamics simulation of smHDAC8. In addition to the standard MD simulations, the recently developed biasing potential replica exchange method was used to enhance the conformational sampling during MD simulation. Our MD simulations suggested that residues in the active site are fairly flexible. Catalytically important residues are highly stable and well preserved their interaction with the zinc ion at the end of the active site tunnel. Simulation shows that residues Tyr341, Phe151, and Lys20 show increased flexibility and detailed analysis of simulation trajectories revealed that these residues adopt two major conformations, one being the conformation similar to that of its human counterpart and the other being schistosome specific (Phe151 and Lys20). Thus, conformational flexibility inferred from MD simulations together with the single substitution identified at the rim of the smHDAC8 pocket represent promising differences between the human and schistosome enzymes.

The *in vitro* characterization of the most interesting compounds was performed with an acetylated peptidic substrate (Fluor de Lys), which led to lower IC₅₀ values than testing with the trifluoroacetyl lysine mimic ZMTFAL. However, as this was a general trend that could also be observed for our reference inhibitors (SAHA and M344), we nevertheless could show that this cost-effective small molecule

substrate can be used at least for pretesting of bigger compound libraries.

Taken together our results provide a framework for specifically targeting a parasitic epigenetic target to cure parasitic diseases by combining structure-based virtual screening with biochemical and *in vivo* studies. Moreover, molecular dynamics combined with ligand docking revealed schistosome specific active site flexibility and this observation is of paramount importance for the design of smHDAC8 specific inhibitors. These results pave the way for similar studies on other major parasites that causes malaria, leishmaniasis, and trypanosomiasis.

■ ASSOCIATED CONTENT

§ Supporting Information

Figure S1: Structure-based sequence alignment of schistosome (*S. mansoni*, *S. japonicum*, *S. hematobium*) and human HDAC8 proteins. Figure S2: Root mean square deviation (Rmsd) of smHDAC8 conformations sampled during MD simulation. Figure S3: Superposition of humanHDAC8 cocrystal structures. Figure S4: Docking pose of OSSL148947 (green carbon atoms) with the homology model of smHDAC8. This material is available free of charge via the Internet at <http://pubs.acs.org>.

■ AUTHOR INFORMATION

Corresponding Author

*Phone: +49-345-55-25040. Fax: +49-345-55-27355. E-mail: wolfgang.sippl@pharmazie.uni-halle.de.

Present Address

[#]Bioinformatics Institute (A*STAR), 30 Biopolis Street, #07-01 Matrix, Singapore 138671, Singapore.

Notes

The authors declare no competing financial interest.

■ ACKNOWLEDGMENTS

This work and the authors of this manuscript received funding from the European Union's Seventh Framework Programme for research, technological development, and demonstration under grant agreements nos. 241865 (SEtTReND) and 602080 (A-ParaDDisE). We thank Anja Kuberski and Inka Negwer for technical assistance. The work of C.R. and M.M. was supported by institutional funds from the Centre National de la Recherche Scientifique (CNRS), the Institut National de la Santé et de la Recherche Médicale (INSERM), and the Université de Strasbourg. This work was supported by the French Infrastructure for Integrated Structural Biology (FRISBI) ANR-10-INSB-05-01 and Instruct as part of the European Strategy Forum on Research Infrastructures (ESFRI).

■ REFERENCES

- (1) Brown, M. Schistosomiasis. *Clin. Med.* **2011**, *11*, 479–482.
- (2) Ross, A. G.; Bartley, P. B.; Sleigh, A. C.; Olds, G. R.; Li, Y.; Williams, G. M.; McManus, D. P. Schistosomiasis. *N. Engl. J. Med.* **2002**, *346*, 1212–1220.
- (3) Gray, D. J.; Ross, A. G.; Li, Y. S.; McManus, D. P. Diagnosis and management of schistosomiasis. *BMJ* **2011**, DOI: 10.1136/bmj.d2651.
- (4) Dömling, A.; Khoury, K. Praziquantel and Schistosomiasis. *ChemMedChem* **2010**, *5*, 1420–1434.
- (5) Ismail, M.; Botros, S.; Metwally, A.; William, S.; Farghally, A.; Tao, L. F.; Day, T. A.; Bennett, J. L. Resistance to praziquantel: direct evidence from *Schistosoma mansoni* isolated from Egyptian villagers. *Am. J. Trop. Med. Hyg.* **1999**, *60*, 932–5.

- (6) Doenhoff, M. J.; Kusel, J. R.; Coles, G. C.; Cioli, D. Resistance of *Schistosoma mansoni* to praziquantel: is there a problem? *Trans. R. Soc. Trop. Med. Hyg.* **2002**, *96*, 465–469.
- (7) Doenhoff, M. J.; Cioli, D.; Utzinger, J. Praziquantel: mechanisms of action, resistance and new derivatives for schistosomiasis. *Curr. Opin. Infect. Dis.* **2008**, *21*, 659–67.
- (8) Norton, A. J.; Gower, C. M.; Lamberton, P. H.; Webster, B. L.; Lwambo, N. J.; Blair, L.; Fenwick, A.; Webster, J. P. Genetic consequences of mass human chemotherapy for *Schistosoma mansoni*: population structure pre- and post-praziquantel treatment in Tanzania. *Am. J. Trop. Med. Hyg.* **2010**, *83*, 951–7.
- (9) Hotez, P. J.; Pecoul, B. “Manifesto” for advancing the control and elimination of neglected tropical diseases. *PLoS Negl. Trop. Dis.* **2010**, *4*, e718.
- (10) Wolffe, A. P.; Matzke, M. A. Epigenetics: regulation through repression. *Science* **1999**, *286*, 481–486.
- (11) Biel, M.; Wascholowski, V.; Giannis, A. Epigenetics – an epicenter of gene regulation: histones and histone-modifying enzymes. *Angew. Chem., Int. Ed. Engl.* **2005**, *44*, 3186–3216.
- (12) Schaefer, S.; Jung, M. Chromatin modifications as targets for new anticancer drugs. *Arch. Pharm. (Weinheim)* **2005**, *338*, 347–357.
- (13) Strahl, B. D.; Allis, C. D. The language of covalent histone modifications. *Nature* **2000**, *403*, 41–5.
- (14) Pierce, R. J.; Dubois-Abdesselem, F.; Lancelot, J.; Andrade, L.; Oliveira, G. Targeting schistosome histone modifying enzymes for drug development. *Curr. Pharm. Des.* **2012**, *18*, 3567–78.
- (15) Andrews, K. T.; Haque, A.; Jones, M. K. HDAC inhibitors in parasitic diseases. *Immunol. Cell Biol.* **2012**, *90*, 66–77.
- (16) Ouaissi, M.; Ouaissi, A. Histone Deacetylase Enzymes as Potential targets in cancer and parasitic disease. *J. Biomed. Biotechnol.* **2006**, *2*, 1–10.
- (17) Grunstein, M. Histone acetylation in chromatin structure and transcription. *Nature* **1997**, *389*, 349–352.
- (18) Peserico, A.; Simone, C. Physical and functional HAT/HADC interplay regulates protein acetylation balance. *J. Biomed. Biotechnol.* **2011**, *371832*.
- (19) Yang, X. J.; Seto, E. The Rpd3/Hda1 family of lysine deacetylases: from bacteria and yeast to mice and men. *Nat. Rev. Mol. Cell Biol.* **2008**, *9*, 206–218.
- (20) North, B. J.; Verdin, E. Sirtuins: Sir2-related NAD-dependent protein deacetylases. *Genome Biol.* **2004**, *5*, 224.
- (21) Cho, Y. S.; Whitehead, L.; Li, J.; Chen, C. H.; Jiang, L.; Vögtle, M.; Francotte, E.; Richert, P.; Wagner, T.; Traebert, M.; Lu, Q.; Cao, X.; Dumotier, B.; Fejzo, J.; Rajan, S.; Wang, P.; Yan-Neale, Y.; Shao, W.; Atadja, P.; Shultz, M. Conformational refinement of hydroxamate-based histone deacetylase inhibitors and exploration of 3-piperidin-3-yldole analogues of dacinostat (LAQ824). *J. Med. Chem.* **2010**, *53*, 2952–2963.
- (22) Marks, P.; Rifkind, R. A.; Richon, V. M.; Breslow, R.; Miller, T.; Kelly, W. K. Histone deacetylases and cancer: causes and therapies. *Nat. Rev. Cancer* **2001**, *1*, 194–202.
- (23) Ito, K.; Ito, M.; Elliott, W. M.; Cosio, B.; Caramori, G.; Kon, O. M.; Barczyk, A.; Hayashi, S.; Adcock, I. M.; Hogg, J. C.; Barnes, P. J. Decreased histone deacetylase activity in chronic obstructive pulmonary disease. *N. Engl. J. Med.* **2005**, *352*, 1967–1976.
- (24) Mukherjee, P.; Pradhan, A.; Shah, F.; Tekwani, B. L.; Avery, M. Structural insights into the *Plasmodium falciparum* histone deacetylase 1 (PfHDAC-1): A novel target for the development of antimalarial therapy. *Bioorg. Med. Chem.* **2008**, *16*, 5254–5265.
- (25) Duvic, M.; Talpur, R.; Ni, X.; Zhang, C.; Hazarika, P.; Kelly, C.; Chiao, J. H.; Reilly, J. F.; Ricker, J. L.; Richon, V. M.; Frankel, S. R. Phase 2 trial of oral vorinostat (suberoylanilide hydroxamic acid, SAHA) for refractory cutaneous T-cell lymphoma (CTCL). *Blood* **2007**, *109*, 31–39.
- (26) Giannini, G.; Cabri, W.; Fattorusso, C.; Rodriguez, M. Histone deacetylase inhibitors in the treatment of cancer: overview and perspectives. *Future Med. Chem.* **2012**, *4*, 1439–1460.
- (27) Andrews, K. T.; Walduck, A.; Kelso, M. J.; Fairlie, D. P.; Saul, A.; Parsons, P. G. Anti-malarial effect of histone deacetylase inhibitors and mammalian tumour cytodifferentiating agents. *Int. J. Parasitol.* **2000**, *30*, 761–768.
- (28) Oger, F.; Dubois, F.; Caby, S.; Noël, C.; Cornette, J.; Bertin, B.; Capron, M.; Pierce, R. J. The class I histone deacetylases of the platyhelminth parasite *Schistosoma mansoni*. *Biochem. Biophys. Res. Commun.* **2008**, *377*, 1079–1084.
- (29) Dubois, F.; Caby, S.; Oger, F.; Cosseau, C.; Capron, M.; Grunau, C.; Dissous, C.; Pierce, R. J. Histone deacetylase inhibitors induce apoptosis, histone hyperacetylation and up-regulation of gene transcription in *Schistosoma mansoni*. *Mol. Biochem. Parasitol.* **2009**, *168*, 7–15.
- (30) Pierce, R. J.; Dubois-Abdesselem, F.; Caby, S.; Trolet, J.; Lancelot, J.; Oger, F.; Bertheaume, N.; Roger, E. Chromatin regulation in schistosomes and histone modifying enzymes as drug targets. *Mem. Inst. Oswaldo Cruz* **2011**, *106*, 794–801.
- (31) Marek, M.; Kannan, S.; Hauser, A. T.; Moraes Mourão, M.; Caby, S.; Cura, V.; Stolfa, D. A.; Schmidtkunz, K.; Lancelot, J.; Andrade, L.; Renaud, J. P.; Oliveira, G.; Sippl, W.; Jung, M.; Cavarelli, J.; Pierce, R. J.; Romier, C. Structural Basis for the Inhibition of Histone Deacetylase 8 (HDAC8), a Key Epigenetic Player in the Blood Fluke *Schistosoma mansoni*. *PLoS Pathog.* **2013**, *9*, e1003645.
- (32) Stolfa, D. A.; Marek, M.; Lancelot, J.; Hauser, A. T.; Walter, A.; Leproult, E.; Melesina, J.; Rumpf, T.; Wurtz, J. M.; Cavarelli, J.; Sippl, W.; Pierce, R. J.; Romier, C.; Jung, M. Molecular basis for the anti-parasitic activity of a mercaptoacetamide derivative that inhibits histone deacetylase 8 (HDAC8) from the human pathogen *Schistosoma mansoni*. *J. Mol. Biol.* **2014**, *426* (20), 3442–3453, DOI: 10.1016/j.jmb.2014.03.007.
- (33) Somoza, J. R.; Skene, R. J.; Katz, B. A.; Mol, C.; Ho, J. D.; Jennings, A. J.; Luong, C.; Arvai, A.; Buggy, J. J.; Chi, E.; Tang, J.; Sang, B. C.; Verner, E.; Wynands, R.; Leahy, E. M.; Dougan, D. R.; Snell, G.; Navre, M.; Knuth, M. W.; Swanson, R. V.; McRee, D. E.; Tari, L. W. Structural Snapshots of Human HDAC8 Provide Insights into the Class I Histone Deacetylases. *Structure* **2004**, *12*, 1325–34.
- (34) Sali, A.; Blundell, T. L. Comparative protein modelling by satisfaction of spatial restraints. *J. Mol. Biol.* **1993**, *234*, 779–815.
- (35) Bürli, R. W.; Luckhurst, C. A.; Aziz, O.; Matthews, K. L.; Yates, D.; Lyons, K. A.; Beconi, M.; McAllister, G.; Breccia, P.; Stott, A. J.; Penrose, S. D.; Wall, M.; Lamers, M.; Leonard, P.; Müller, I.; Richardson, C. M.; Jarvis, R.; Stones, L.; Hughes, S.; Wishart, G.; Haughan, A. F.; O’Connell, C.; Mead, T.; McNeil, H.; Vann, J.; Mangette, J.; Maillard, M.; Beaumont, V.; Munoz-Sanjuan, I.; Dominguez, C. Design, synthesis, and biological evaluation of potent and selective Class IIa histone deacetylase (HDAC) inhibitors as a potential therapy for Huntington’s disease. *J. Med. Chem.* **2013**, *56*, 9934–9954.
- (36) Case, D. A.; Darden, T. A.; Cheatham, T. E., III; Simmerling, C. L.; Wang, J.; Duke, R. E.; Luo, R.; Walker, R. C.; Zhang, W.; Merz, K. M.; Roberts, B.; Wang, B.; Hayik, S.; Roitberg, A.; Seabra, G.; Kolossaváry, I.; Wong, K. F.; Paesani, F.; Vanicek, J.; Liu, J.; Wu, X.; Brozell, S. R.; Steinbrecher, T.; Gohlke, H.; Cai, Q.; Ye, X.; Wang, J.; Hsieh, M. J.; Cui, G.; Roe, D. R.; Mathews, D. H.; Seetin, M. G.; Sagui, C.; Babin, V.; Luchko, T.; Gusarov, S.; Kovalenko, A.; Kollman, P. A. AMBER 11; University of California, San Francisco, 2010.
- (37) Jorgensen, W. L.; Chandrasekhar, J.; Madura, J. D.; Impey, R. W.; Klein, M. L. Comparison of simple potential functions for simulating liquid water. *J. Chem. Phys.* **1983**, *79*, 926–935.
- (38) Duan, Y.; Wu, C.; Chowdhury, S.; Lee, M. C.; Xiong, G.; Zhang, W.; Yang, R.; Cieplak, P.; Luo, R.; Lee, T.; Caldwell, J.; Wang, J.; Kollman, P. Point charge force field for molecular mechanics simulations of proteins based on condensed-phase quantum mechanical calculations. *J. Comput. Chem.* **2003**, *24*, 1999–2012.
- (39) Pang, Y. P. Novel zinc protein molecular dynamics simulations: Steps toward antiangiogenesis for cancer treatment. *J. Mol. Model.* **1999**, *5*, 196–202.
- (40) Darden, T.; York, D.; Pedersen, L. Particle mesh Ewald: An $N_{\log}(N)$ method for Ewald sums in large systems. *J. Chem. Phys.* **1993**, *98*, 10089–10092.

- (41) Miyamoto, S.; Kollman, P. A. Settle: An analytical version of the SHAKE and RATTLE algorithm for rigid water models. *J. Comput. Chem.* **1992**, *13*, 952–962.
- (42) Kannan, S.; Zacharias, M. Enhanced sampling of peptide and protein conformations using replica exchange simulations with a peptide backbone biasing-potential. *Proteins* **2007**, *66*, 697–706.
- (43) Schrödinger Suite 2012, Maestro version 9.3, Protein Preparation Wizard, Epik version 2.3, Glide version 5.8, Schrödinger, LLC: New York, 2012.
- (44) Irwin, J. J.; Sterling, T.; Mysinger, M. M.; Bolstad, E. S.; Coleman, R. G. ZINC: A Free Tool to Discover Chemistry for Biology. *J. Chem. Inf. Model.* **2012**, *52*, 1757–1768.
- (45) Friesner, R. A.; Murphy, R. B.; Repasky, M. P.; Frye, L. L.; Greenwood, J. R.; Halgren, T. A.; Sanschagrin, P. C.; Mainz, D. T. Extra Precision Glide: Docking and Scoring Incorporating a Model of Hydrophobic Enclosure for Protein–Ligand Complexes. *J. Med. Chem.* **2006**, *49*, 6177–6196.
- (46) Jones, G.; Willett, P.; Glen, R. C.; Leach, A. R.; Taylor, R. Development and validation of a genetic algorithm for flexible docking. *J. Mol. Biol.* **1997**, *267*, 727–748.
- (47) Baxter, C. A.; Murray, C. W.; Clark, D. E.; Westhead, D. R.; Eldridge, M. D. Flexible docking using Tabu search and an empirical estimate of binding affinity. *Proteins* **1998**, *33*, 367–382.
- (48) Mooij, W. T. M.; Verdonk, M. L. General and Targeted Statistical Potentials for Protein–Ligand Interactions. *Proteins: Struct. Funct. Bioinf.* **2005**, *61*, 72–287.
- (49) Stützle, K. T.; Exner, T. E. Empirical Scoring Functions for Advanced Protein–Ligand Docking with PLANTSO. *J. Chem. Inf. Model.* **2009**, *49*, 84–96.
- (50) Heltweg, B.; Dequiedt, F.; Marshall, B. L.; Brauch, C.; Yoshida, M.; Nishino, N.; Verdin, E.; Jung, M. Subtype selective substrates for histone deacetylases. *J. Med. Chem.* **2004**, *47*, 5235–5243.
- (51) Park, H.; Kim, S.; Kim, Y.; Lim, S. J. A Structure-Based Virtual Screening Approach toward the Discovery of Histone Deacetylase Inhibitors: Identification of Promising Zinc-Chelating Groups. *Chem. Med. Chem.* **2010**, *5*, 591–597.
- (52) Hildmann, C.; Wegener, D.; Riester, D.; Hempel, R.; Schober, A.; Merana, J.; Giurato, L.; Guccione, S.; Nielsen, T. K.; Ficner, R.; Schwienhorst, A. Substrate and inhibitor specificity of class 1 and class 2 histone deacetylases. *J. Biotechnol.* **2006**, *124*, 258–270.
- (53) Krennhrubec, K.; Marshall, B. L.; Hedglin, M.; Verdin, E.; Ulrich, S. M. Design and evaluation of ‘Linkerless’ hydroxamic acids as selective HDAC8 inhibitors. *Bioorg. Med. Chem. Lett.* **2007**, *17*, 2874–8.